Microgravity Science and Technology (2020) 32:587–596
https://doi.org/10.1007/s12217-020-09801-3

ORIGINAL ARTICLE

Liquid Sloshing in Partially Filled Capsule Storage Tank Undergoing Gravity Reduction to Low/Micro-Gravity Condition

Ji-Cheng LI[1,2] · Hai LIN[1] · Kai LI[1,2] · Jian-Fu ZHAO[1,2] · Wen-Rui HU[1]

Received: 24 October 2019 / Accepted: 3 May 2020 / Published online: 10 June 2020

Abstract

Liquid sloshing in storage tanks is of critical concern for the fluid management in space. In the present study, oscillation of liquid in a partially filled capsule storage tank was numerically studied using the volume of fluid method and taking into account the dynamic contact angle. The filling ratios of tank ranging from 10% to 90% and the gravity levels of 10^{-3} g_0 and 0 g_0 were considered as the controlling variables. The temporal evolution of characteristic points of free surface and the law of oscillation frequencies were analyzed. The results show that for different filling ratios, the oscillations of free surfaces present different damping types, in which the small and large filling ratios correspond to the underdamping and the intermediate filling ratios to the critical damping. The present study provides fundamental insights into the free surface oscillations depending on the filling ratios and residual gravity level, which is useful for the corresponding utilization in space.

Keywords Liquid sloshing · Tank · Low/micro gravity · VOF method · Contact angle

Introduction

Propellant storage tank is one of the key components in a spacecraft system. Liquid sloshing in the tanks significantly affects the ability of propellant support, stability and safety of system (Dalmon et al. 2018). Most studies on the subject concentrated on the pitching or stimulating effects in terrestrial condition, e.g. Zhao et al. 2018, Sanapala et al. 2018, Frosina et al. 2018. What researchers concerned is fuels, chemical fluids and so on, which is easy to be disturbed (Wang et al. 2017) and to interact with the structures. However, the liquid sloshing in storage tanks in space exhibits more complexity comparing with the terrestrial condition. In 1999, the Sloshsat FLEVO project was conducted to investigate the liquid behavior in spacecraft (Vreeburg 1999). The tank in the experiment is a cylinder configuration with hemispherical ends, which is mostly used in today's spacecraft. Later, numerical simulation was carried out on the coupling solid-liquid dynamics (Luppes et al. 2009), where the volume of fluid (VOF) method (Gueyffier 1999; Hirt 1981) was adopted to capture the free surface evolution. The Parabolic Flight was used by Fernandez et al. (2017).to investigate the potentially complex behaviour of vibrated liquids in weightless environments.

In regard to the fluid sloshing inside a tank under normal gravity condition, the interactions between solid structure and liquid sloshing were widely discussed, e.g. Chiba and Magata 2017, Ohayon and Soize 2015. The relations between free surface oscillation frequencies, fill depths and radius ratios were studied by Hasheminejad and Soleimani. They found that the oscillation frequencies increased as the fill depth approached near-empty and near-full condition as well as corresponded with its oscillation modes (Hasheminejad and Soleimani 2017). Zhang et al. developed an augmented incompressible material point method to model liquid sloshing problems and validated it in a rectangular sloshing tank (Zhang et al. 2018). The potential flow theory was also

This article belongs to the Topical Collection: Multiphase Fluid Dynamics in Microgravity
Guest Editors: Tatyana P. Lyubimova, Jian-Fu Zhao

✉ Kai LI
likai@imech.ac.cn

✉ Jian-Fu ZHAO
jfzhao@imech.ac.cn

[1] Key Laboratory of Microgravity (National Microgravity Laboratory), Institute of Mechanics, Chinese Academy of Sciences, Beijing 100190, China

[2] School of Engineering Science, University of Chinese Academy of Sciences, Beijing 100049, China

applied to investigate the dynamic response and motion of fluid inside a container induced by arbitrary combination of lateral, longitudinal, and rotational excitations (Dai et al. 2019; Han et al. 2019). These research works provide valuable methods and meaningful results of liquid sloshing inside tanks. However, when it comes to the low/micro gravity conditions in space, the capillary effect, which was not considered in aforementioned researches, play a leading role in the liquid behavior in storage tank.

Generally speaking, there are two types of free surface modelling method (Scardovelli and Zaleski 1999): capturing method based on the Eulerian system, such as VOF and Level Set method, and tracking method based on the Lagrangian system, such as Marker method (Popinet and Zaleski 1998). Dalmon et al. used the Level Set method coupled with the Ghost Fluid Method simulated liquid sloshing in spherical tanks and compared with the results of the FLUIDICS experiment carried out in the International Space Station (ISS) (Dalmon et al. 2019). In the study, the force and torque exerted by fluids on the tank wall under different angular velocity and angular acceleration conditions were investigated. It shows that the oscillation frequency of bubble inside the tank increases with the angular velocity. Li et al. conducted experimental research about the dynamic behaviors of liquid in partially filled tank in short-term micro-gravity condition on the Drop Tower Beijing and carried out corresponding numerical simulation using the VOF method (Li et al. 2018). Yang et al. conducted numerical simulations about the nonlinear liquid sloshing with angle and angular pitching in micro-gravity condition using the VOF method, in which the relation between filling level and sloshing frequency was analyzed (Yang et al. 2019). Utsumi studied the damping effect of contact angle hysteresis in a spherical storage tank in low-gravity condition and found that the damping ratio could reach the same order as the viscous damping ratio for low Bond numbers due to the nonlinear effect of contact angle hysteresis (Utsumi 2017). Moreover, the damping ratio is higher for large than low filling levels under a very small Bond number. With respected to the fluid sloshing and external excitations, Miao et al. proposed an equivalent mechanical model of large amplitude fluid sloshing in a tank subjected to external lateral excitations in low-gravity condition (Miao et al. 2017). Deng and Yue focused the attitude tracking control of the spacecraft with large sloshing amplitude (Deng and Yue 2017).

For most of the numerical studies on liquid sloshing inside a storage tank in low/micro-gravity condition, as aforementioned, the DCA model was not taken into account. Nevertheless, the contact angle hysteresis plays an important role in the free surface evolution comparing with the static contact angle model (Stange et al. 2003). Researches about dynamic contact angle (DCA), caused by contact angle hysteresis, were basically focused on the spreading of liquids on solid surfaces as Cox systematically discussed (Cox 1986). The relationship between DCA and the moving contact line (MCL) is what matters (Snoeijer and Andreotti 2013; Sui et al. 2014). Numerous researches involving the MCL or interface problems have adopted different DCA model to their detailed works, such as the droplet impact on surface in supercooled environment (Chang et al. 2019), the droplet behaviors in microchannel (Wang et al. 2019), the splashing of droplet onto a surface (Almohammadi and Amirfazli 2019; Quetzeri-Santiago et al. 2019). In addition, Blake and Batts experimentally investigated the relation between temperature and DCA, and the results showed that the effects of temperature on DCA were not restricted to affect the surface tension and viscosity (Blake and Batts 2019). Fricke et al. theoretically analyzed the MCL problem for two-phase incompressible flows with a kinematic approach and found that the derivative of the contact angle was in terms of the velocity gradient at the solid wall (Fricke et al. 2019). Viola et al. incorporated a nonlinear contact line model where a steep dynamic hysteresis range was adopted into asymptotic analysis of the sloshing dynamics in a circular cylinder in partial wetting conditions (Viola et al. 2018). It is shown that the damping effect of contact line was nonlinearly depended on the amplitude of motion. Our recent numerical simulations also verified the importance of DCA in the study of the free surface evolutions of liquid sloshing in a modeled half capsule tank.

As is clear from the above descriptions, the DCA model is of great importance for the dynamic behaviors of liquid in low Bond numbers. However, few previous studies has considered the DCA model as a factor influencing liquid sloshing in a tank. Our objective is to focus on what influence the DCA model will perform on liquid sloshing combining the factors of filling ratio and gravity level. In present study, numerical simulations on the liquid sloshing in partially filled capsule storage tanks were conducted taking the DCA model (Kistler 1993) into consideration. The liquid sloshing laws in the storage tanks in low/micro-gravity condition were investigated in details, and effects of the dynamic contact angle on the liquid sloshing laws were also discussed.

Physical Model and Numerical Method

Physical and Numerical Models

As shown in Fig.1, a scaled capsule storage tank model filled with the liquid ethanol and its vapor was chosen in the present study, and the assumption of an axisymmetric domain was adopted. The originate coordinate is located at the midplane of the tank.

The governing equations for two-phase flow are as follows.

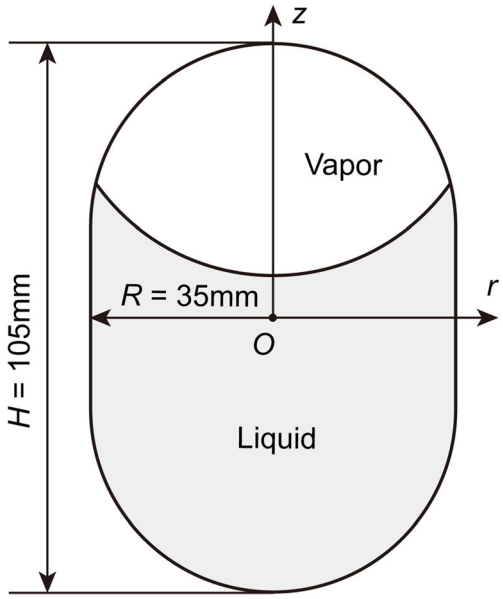

Fig. 1 Physical model of the capsule storage tank

The conservative governing equation of volume fraction:

$$\frac{\partial \alpha}{\partial t} + \nabla\cdot(\mathbf{u}\alpha) = 0 \tag{2.1}$$

where α is the volume fraction in the calculation domain. Considering the low flow velocity of the inner flow field, the fluid can be treated as incompressible. Therefore, the volume fraction eq. (2.1) is reduced to the nonconservative form

$$\frac{\partial \alpha}{\partial t} + \mathbf{u}\cdot\nabla\alpha = 0 \tag{2.2}$$

The continuity equation and momentum conservation equations are:

$$\frac{\partial \rho}{\partial t} + \nabla\cdot(\rho\mathbf{u}) = 0 \tag{2.3}$$

$$\frac{\partial(\rho\mathbf{u})}{\partial t} + \nabla\cdot(\rho\mathbf{u}\mathbf{u}) = -\nabla p + \nabla\cdot\boldsymbol{\tau} + \rho\mathbf{g} + \mathbf{f}_s \tag{2.4}$$

where the volume force caused by the surface tension is $\mathbf{f}_s = 2\sigma_{ij}\rho\kappa_i\nabla\alpha_i/(\rho_i+\rho_j)$, in which $\kappa_i$is the curvature calculated by the gradients of the unit normal vector of the phase interface as $\kappa = -\nabla\cdot\hat{\mathbf{n}}$. The unit normal vector $\hat{\mathbf{n}}$ is calculated by $\hat{\mathbf{n}} = \nabla\alpha/|\nabla\alpha|$. The stress tensor $\boldsymbol{\tau} = (\lambda\nabla\cdot\mathbf{u})I + 2\mu\mathbf{D}(\mathbf{u})$, in which the strain tensor $\mathbf{D}(\mathbf{u}) = (\nabla\mathbf{u} + \nabla\mathbf{u}^T)/2$, and the second viscosity coefficient $\lambda = -\frac{2}{3}\mu$, $\mu$is the viscosity of fluids. Note that the parameters in the governing equations are treated as weighted quantities of two-phase in a form of $x = \alpha x_1 + (1-\alpha)x_2$, both for ρ and μ.

No slip condition was applied on the internal solid wall boundary of the tank. The detailed mathematical form is as follows:

$$\mathbf{u}\cdot\hat{\mathbf{n}}_w = 0, \quad \mathbf{u}_\parallel = 0, \quad \left.\frac{\partial p}{\partial n}\right|_w = 0, \quad \left.\frac{\partial \alpha}{\partial n}\right|_w = 0 \tag{2.5}$$

where $\mathbf{u}_\parallel$is the velocity tangent to the wall, $\hat{\mathbf{n}}_w$ is the unit vector normal to the wall. The last two equations in (2.5) is the normal gradient to the solid wall.

The effect of contact angle is described by the wall adhesion model in following form (Brackbill et al. 1992):

$$\hat{\mathbf{n}} = \hat{\mathbf{n}}_w\cos\theta_w + \hat{\mathbf{t}}_w\sin\theta_w \tag{2.6}$$

where $\hat{\mathbf{t}}_w$ is the unit vector tangential to the wall. θ_w is the contact angle, i.e. the dynamic contact angle θ_D.

In the present study, ethanol (C_2H_5OH) was chosen to be the working fluid in the numerical simulations. The properties of ethanol are shown in Table 1 (data from NIST). The equilibrium states of liquid in the partially filled capsule tank in terrestrial condition were calculated as the initial conditions for the numerical simulation. Here the gravity acceleration, $g_0 = 9.81$ m/s^2, is adopted for the terrestrial condition, 10^{-3} g_0 for the low-gravity condition, and 0 for the microgravity condition. The corresponding dimensionless Bond numbers,$Bo = (\rho_l - \rho_g)gl^2/\sigma$, are 0.41 and 0, where ρ_l and ρ_g stand for the densities of liquid and vapor (gas).

DCA Assumption Model

Dynamic contact angle model considering the contact angle hysteresis originates from the difference between ideal and real surfaces. It shows a type of saturation function of the contact angle with capillary number. The curve of dynamic contact angle of ethanol are shown in Fig. 2. The model of Hoffman (Hoffman 1975) is

$$\theta_D^3 - \theta_e^3 = c_T Ca \tag{2.7}$$

for a small Ca ($4\times10^{-5} < Ca < 36$), where $Ca = \mu V/\sigma$. Jiang et al. proposed an empirical correlation (Jiang et al. 1979) as

$$\frac{\cos\ (\theta_e) - \cos\ (\theta_D)}{\cos\ (\theta_e) + 1} = \tanh\left(4.96Ca^{0.702}\right) \tag{2.8}$$

And Kistler (Kistler 1993) proposed a derived DCA formula as

Table 1 The parameters of C_2H_5OH

Materials	ρ (kg/m^3)	μ(Pa·s)	σ (mN/m)	θ_e (°)
C_2H_5OH(liquid)	790	1.20×10^{-3}	23	1
C_2H_5OH(vapor)	2.06	1.08×10^{-5}		

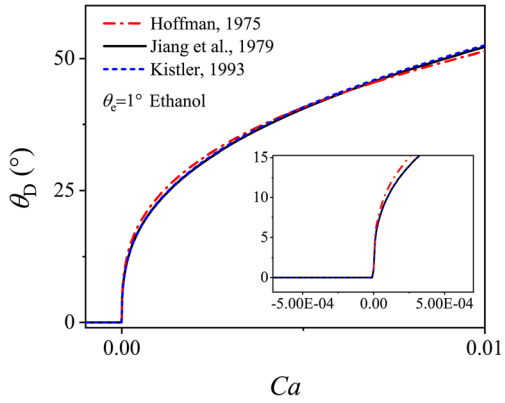

Fig. 2 Dynamic contact angle of ethanol based on three DCA models

$$\theta_D = f_{\text{Hoff}}\left[Ca + f_{\text{Hoff}}^{-1}(\theta_e)\right] \tag{2.9}$$

$$f_{\text{Hoff}}(x) = \arccos\left\{1-2\tanh\left[5.16\left(\frac{x}{1+1.31x^{0.99}}\right)^{0.706}\right]\right\} \tag{2.10}$$

As shown in Fig. 2, there is no significant difference among the models in the present case where Ca is the order of 10^{-3}. So the widely used (Šikalo et al. 2005; Malgarinos et al. 2014) DCA model of Kistler is adopted in present work.

Numerical Method and Grid Independence

The continuum surface force (CSF) model was adopted (Brackbill et al. 1992), which expressed in the form of volume force as show in eq. (2.4) of the $\mathbf{f}_s$. The piecewise-linear interface capture (PLIC) method was used for the reconstruction of the interface (Youngs 1982). To capture the oscillation of free surface evolutions in the storage tank in low/micro-gravity condition, the volume of fluid method (VOF) (Gueyffier 1999; Hirt 1981) was adopted. The Pressure-Implicit with Splitting of Operators (PISO) (Issa 1986) method with skewness-neighbor correction was adopted to couple the pressure and velocity, for the sake of high efficiency of which in transient problems and relatively large time step. The momentum in spatial dimension was discretized in second order upwind scheme, and in temporal the first order implicit scheme was taken into account. Specifically, the pressure in spatial was discretized using the PRESTO scheme with second order accuracy.

Figure 3 shows the grid distribution. The unstructured quadrilateral mesh with refined boundary layers were adopted. To check the independence of grid, the positions of contact line at the equilibrium state in the capsule tank with the filling ratio of 50% in terrestrial condition were calculated based on different grid distributions. As shown in Fig. 4, the equilibrium position of contact line asymptotes to a certain value with the increase of grid number, and the relative error between the

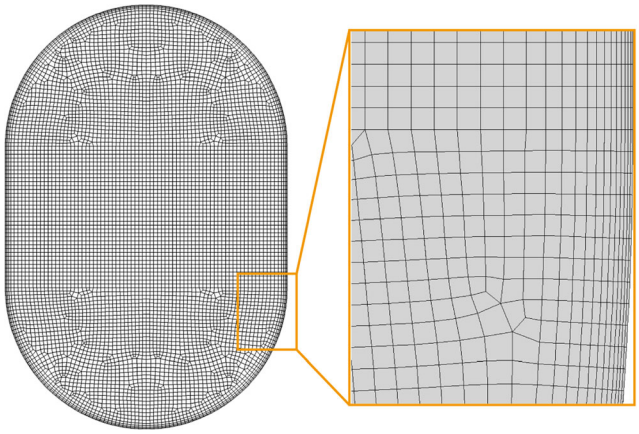

Fig. 3 Grid distribution

grid number 66616 and 134,405 is 1.28%, which is extremely small. Thus, the grid number 66616 was chosen as the grid scheme in subsequent numerical simulation.

Results and Discussion

To describe the liquid sloshing in the capsule storage tank, three important characteristic points were selected, as shown in Fig. 5: the position of the moving contact line (MCL), the position of the free surface center (FSC), and the position of the upper free surface center (FSCup) when the moving contact line merges at the top of tank to form a fully enveloped ullage by the liquid for the case with high filling ratio. The temporal evolutions of the characteristic points are revealed in following sections in details.

Effects of Dynamic Contact Angle Model

To explicitly depict the necessity of considering the dynamic contact angle model in the numerical simulation, the liquid sloshing in a storage tank with the filling ratio 50% in micro-gravity condition was studied considering the DCA model and the static contact angle (SCA) model, respectively. As shown in Fig. 6a, the same initial free surface configuration

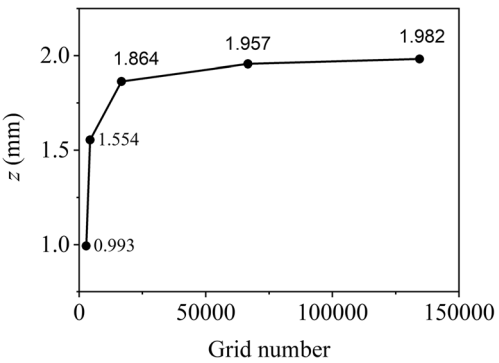

Fig. 4 Grid independence

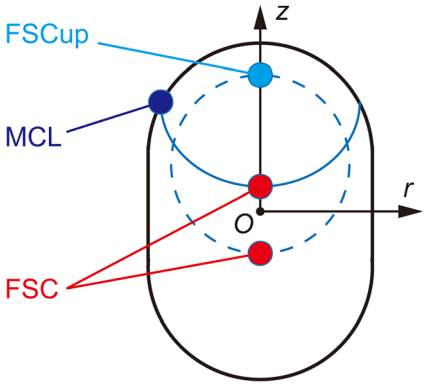

Fig. 5 Characteristic points of the free surface

for both cases is the equilibrium state in terrestrial condition. The free surface is nearly planar except the tiny rising up in the vicinity of contact line. After the step reduction of gravity to micro-gravity condition, the equilibrium free surface configuration in micro-gravity condition is shown in Fig. 6b. The

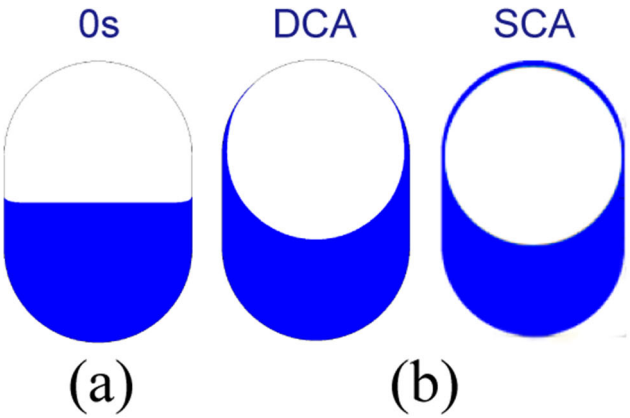

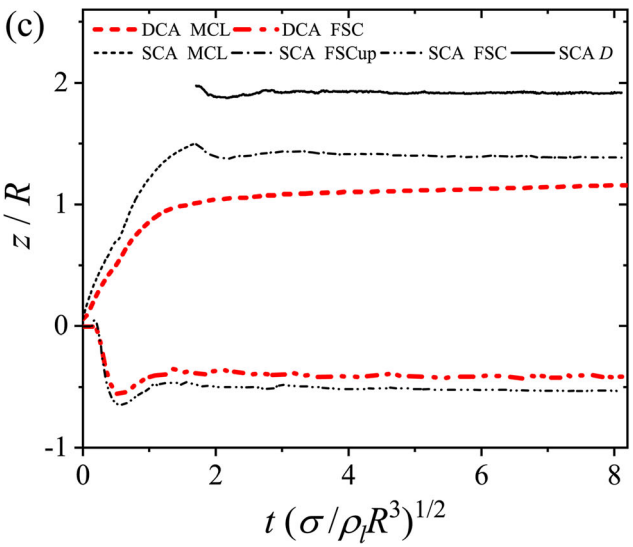

Fig. 6 Comparisons of (a) phase distribution in the tank at 0 s, (b) the equilibrium states of the free surface and (c) temporal evolution of characteristic points in dimensionless form considering DCA and SCA in the storage tank with the filling ratio 50%

ullage is fully enveloped by the liquid for the case with the SCA model while it is only partially enveloped for the case with the DCA model. Figure 6c shows the temporal evolutions of the characteristic points mentioned above. It can be seen that the discrepancies arise right after the beginning of the gravity reduction. The numerical results with the SCA model overpredict not only the moving velocity of the contact line but also both the amplitude and frequency of the free surface oscillation. Moreover, the oscillation of the contact line around the equilibrium position is not observed in the numerical results with the DCA model. By dimensional analysis, two characteristic time scales are derived (Stange et al. 2003): the viscous time scale $t_1 \sim \rho_l R^2/\mu$ and the capillary time scale $t_2 \sim \sqrt{\rho_l R^3/\sigma}$, where R is the characteristic length, the radius of tank here. In present study, the value of the two time scale are $t_1 = 806.46$ s, $t_2 = 1.21$ s. The energy of surface tension $E_\sigma = \sigma/\kappa^2$ is the source of the free surface sloshing. The characteristic velocity due to the capillary effect is of the magnitude $u_{Ca} \sim (\sigma\kappa/\rho)^{1/2}$. When the contact line proceeds, the numerical simulation with the SCA model predicts a larger free surface curvature resulting in a larger characteristic velocity. Moreover, the comparison between the numerical results and Drop Tower experimental results on a partially filled half capsule tank reported elsewhere shows that numerical results with the DCA model are in good agreement with the experimental results in contrast to the case with the SCA model. Therefore, it is crucial to take the DCA model into consideration to accurately predict the liquid sloshing behavior in a partially filled storage tank in the following numerical study.

Dynamic Behavior of Liquid Sloshing

The behavior of the liquid sloshing in partially filled storage tanks significantly depends on the fill ratio and the residual gravity level (Li et al. 2018). Therefore, effects of the filling ratios, ranging from 10% to 90%, on the liquid sloshing in capsule storage tanks were systematically studied in low/micro-gravity condition. Figure 7 shows the dynamic vapor-liquid phase distributions in the capsule tanks during the step reduction of gravity from terrestrial condition to low-gravity condition and micro-gravity condition. Representative filling ratios, 20%, 40%, 60% and 90%, were plotted. Figure 8 shows the corresponding temporal evolutions of the characteristic points, where D is the longitudinal length of the fully enveloped ullage defined as $D = z_{\mathrm{FSCup}} - z_{\mathrm{FSC}}$. For all the cases, the initial free surface configurations in terrestrial condition are qualitatively same. The free surface is nearly planar except the tiny rising up in the vicinity of contact line. The behavior of the characteristic points can be divided into two regimes during the gravity reduction to micro-gravity condition, the short-period regime of rapid movement and the long-period regime to equilibrium position. In the short-period

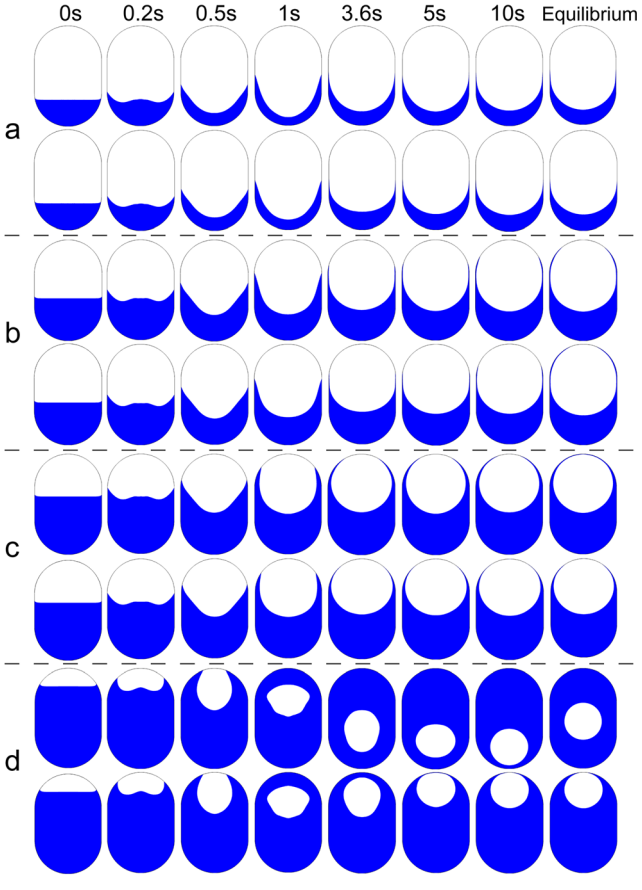

Fig. 7 Dynamic phase distributions in tanks with different filling ratios (a) 20%, (b) 40%, (c) 60% and (d) 90% in micro-gravity condition (top) and low-gravity condition (bottom)

regime of rapid movement, the contact line proceed along the tank while the free surface significantly deviates from the initial configuration. In the long-period regime to equilibrium position, for the cases with low filling ratios, the contact line keeps proceeding acting as a free contact line at a much lower velocity while the free surface undergoes a damped oscillation. The equilibrium position of the contact line increases with the increasing filling ratio. For the cases with high filling ratios, the contact line merges at the top of tank and the ullage is fully enveloped by the liquid. Note that the equilibrium phase distribution in the tank is tended to have the minimum surface energy. For the present isothermal condition, the curvature of equilibrium free surface configuration reaches the maximum value corresponding to a sphere or a part of a sphere in micro-gravity condition. The fully enveloped ullage shifts in the bulk liquid until reaching the equilibrium state that the ullage profile remains a sphere shape unchanged. The oscillations of the upper center and the center of the free surface are strongly coupled as shown in Fig. 7d.

The liquid sloshing during the gravity reduction to low-gravity condition reveal the similar dynamic behaviors of the phase distributions. For the cases with the same filling ratios, in the short-period regime of rapid movement, the moving velocities of the contact line are nearly identical in both the micro-gravity condition and low-gravity condition due to the strong capillary effects. In the long-period regime to equilibrium position, however, the residual gravity of 10^{-3} g_0 counteracts the capillary effect. It results in the lower equilibrium position of contact line for the cases with low filling ratios, and an enveloped ellipsoidal ullage remains on the top of tank due to the buoyancy for the cases with high filling ratios. Hence, the time required to reach the equilibrium state in low-gravity condition is much shorter than that in micro-gravity condition.

Oscillation Frequency Analysis of Liquid Sloshing

The sloshing of the free surface can be described by an one-dimensional mass-spring system,

$$\frac{\partial^2 x}{\partial t^2} + 2\xi\omega_0 \frac{\partial x}{\partial t} + \omega_0^2 x = 0 \tag{3.1}$$

where ω_0 is the inherent angular frequency, ξ the damping ratio and x the displacement from equilibrium position. Three kinds of analytic solutions to the differential equation are as follows:

(a) Underdamping, $\xi < 1$,

$$x(t) = A_0 \exp(-\xi\omega_0 t)\cos(\omega t + \Phi) \tag{3.2}$$

where A_0 is the amplitude of the oscillation, $\omega = \sqrt{1-\xi^2}\omega_0$ the angular frequency, and Φ the initial phase. The damping oscillation is with respect to the equilibrium position determined by the solution eq. (3.2).

(b) Critical damping, $\xi = 1$,

$$x(t) = (A_1 + A_2 t)\exp(-\xi\omega_0 t) \tag{3.3}$$

where A_1 and A_2 are the amplitude of the oscillation. The oscillation only runs across the equilibrium position once and then approaches the equilibrium position.

(c) Overdamping, $\xi > 1$, the oscillation never runs across the equilibrium position. Actually, no oscillation occur in this case.

In the present study, Fast Fourier Transform (FFT) was conducted on the oscillation of the free surface. The typical FFT results of two cases with the filling ratio of 20% and 75 under low-gravity condition are shown as Fig. 9. For the cases with low filling ratios, the data span ranges from the first local maximum of the FSC profile to its equilibrium state. For the cases with high filling ratios, the data span is from the formation of the fully enveloped ullage to its equilibrium state, as shown in Fig. 8. Figure 10 summarized the main oscillation frequencies as a function of the filling ratio. With the gravity reduction to micro-gravity condition, the main frequency

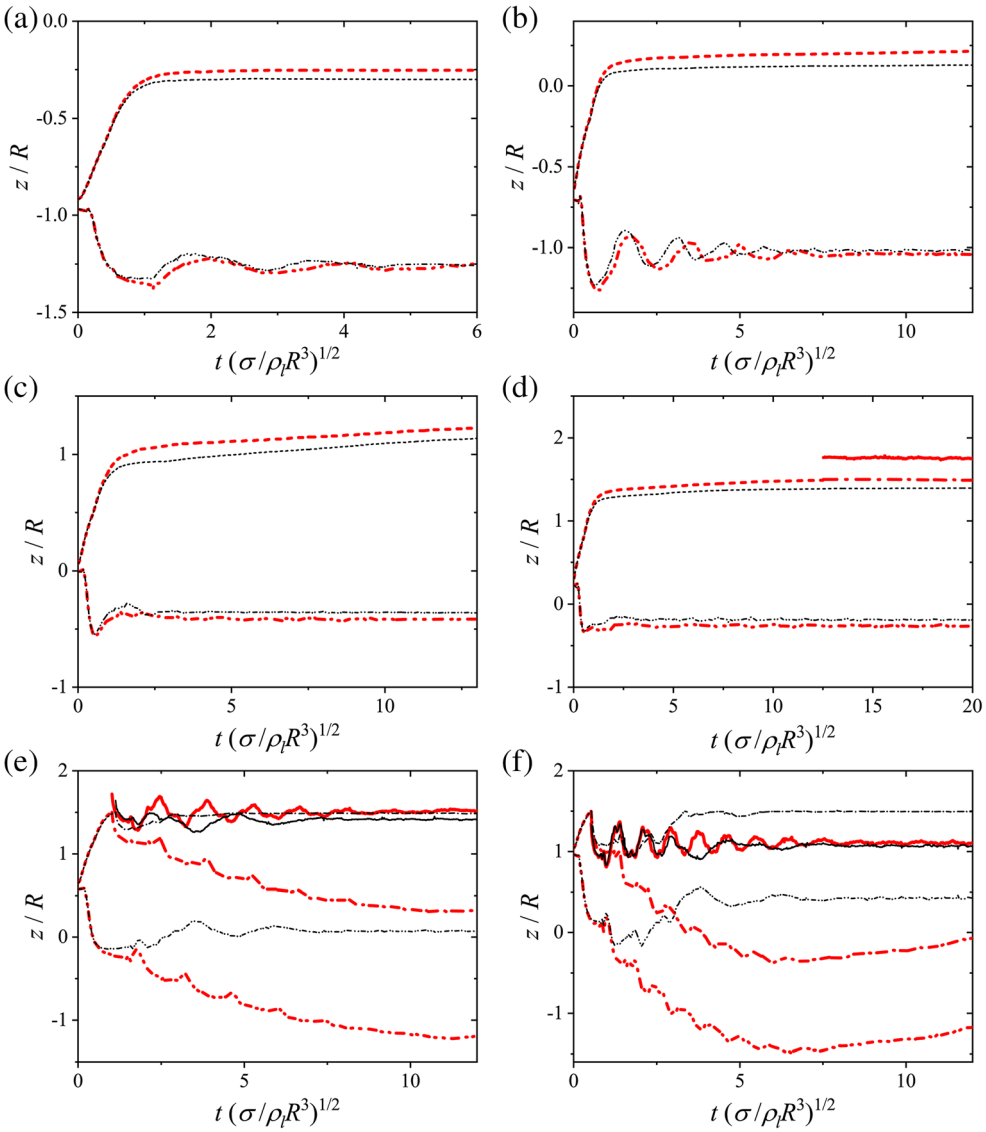

Fig. 8 Temporal evolutions of the characteristic points in the tanks. The filling ratios from *a* to *f* are (a) 10%, (b) 20%, (c) 50%, (d) 60%, (e) 75% and (f) 90%. The different curves represent: MCL (dash), FSCup (dash dot), FSC (dash dot dot), *D* (solid). The red (■) line and black (■) line stands for micro-gravity and low-graivty, respectively

slightly increases with the increasing filling ratio and then nearly keeps constant in the range of low filling ratios. On the other hand, the main frequency shows a rapid increase monotonously with the increasing filling ratio in the range of high filling ratios. They both exhibit the characteristics of the underdamping type. The critical damping type dominates the oscillations in the range of intermediate filling ratios. With the gravity reduction to low-gravity condition, the tendency of the main oscillation frequencies dependent on the filling ratio is similar. However, the residual gravity results in the higher

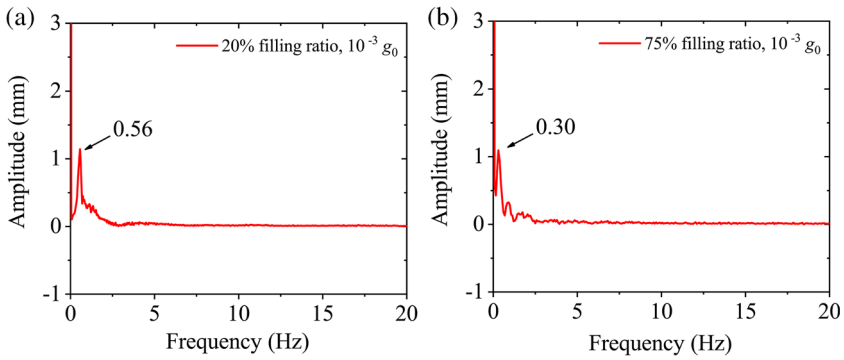

Fig. 9 Typical FFT results of oscillations for the (a) 20% and (b) 75% filling ratios in the 10^{-3} g_0 gravity condition

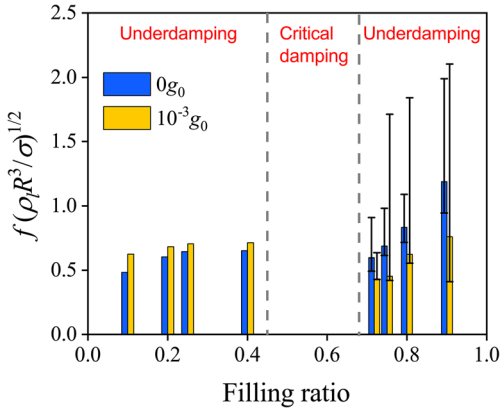

Fig. 10 Frequency analysis of characteristic point oscillations of free surface in tank. The values of bar are the dominant frequencies from FFT. The error bar represents the maximum/minimum local frequencies for the corresponding filling ratios

oscillation frequency in the range of low filling ratios while much lower oscillation frequency in the range of high filling ratios, e.g. the difference is 36% for the case with the filling ratio 90%.

Figure 11 shows the temporal evolutions of the oscillation frequency of each half oscillation period of D for the high filling ratios of 71.8% (In this case, the initial liquid height exactly reaches the tangent line between the upper hemisphere and the cylinder), 75%, 80% and 90%. With the gravity reduction to micro-gravity condition, the frequencies of oscillations nearly hold constant for the cases with filling ratios of 71.8%, 75% and 80%, and decline for the case with filling ratio 90%. However, the oscillation frequencies significantly decrease in low-gravity condition except the cases with filling ratio 71.8% which is neighbor to the critical damping regime. By linear fitting, it is shown that the slopes of the dimensionless frequencies over time in low-gravity condition are 3 ~ 10 times of those in micro-gravity condition.

The frequency of capillary wave is equal to the Rayleigh frequency f_R (Dalmon et al. 2018), defined as

$$f_R = \sqrt{\frac{\sigma}{\rho_l R^3}} = 0.824 \text{ Hz} \tag{3.4}$$

which is equal to the inverse of time scale t_2. The detailed frequency analysis in the present study showed that the liquid sloshing in the tanks is dominated by the capillary effect. From the viewpoint of energy conservation, the reason is that the volume force term $\rho\mathbf{g}$ in eq. (2.4) counteracted part of the surface tension force term $\mathbf{f}_s$, which leads to a longer period occupied by the capillary wave to reach the minimum potential energy of free surface.

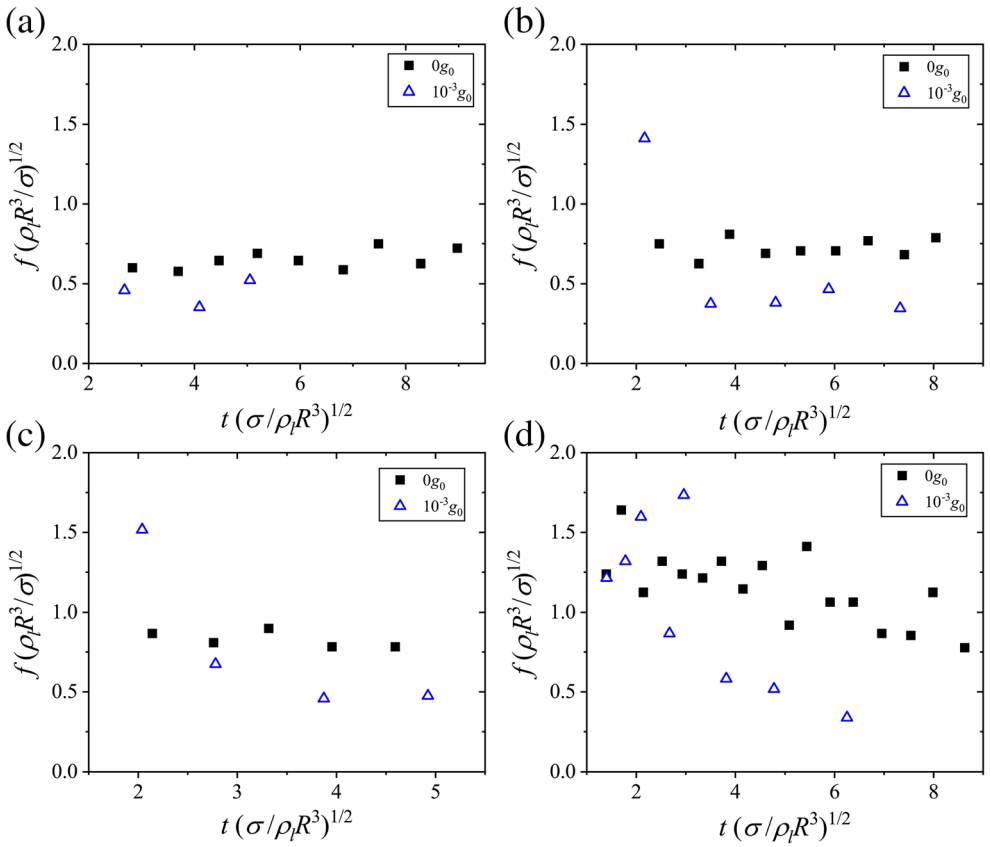

Fig. 11 Temporal evolutions of oscillation frequencies for different filling ratios (a) 71.8%, (b) 75%, (c) 80% and (d) 90%

Conclusion

Liquid sloshing in partially filled capsule storage tanks was numerically investigated. The dynamic contact angle model was taken into account. The results reveal strong influence of the filling ratio and residual gravity level on the dynamic behavior of the free surface. With the gravity reduction to micro-gravity condition, for the cases with low filling ratios, the contact line keeps proceeding acting as a free contact line while the free surface undergoes a damping oscillation to the equilibrium state. The equilibrium position of the contact line increases with the increasing filling ratio. For the cases with high filling ratios, the contact line merges at the top of tank and the ullage is fully enveloped by the liquid shifting in the bulk liquid till the equilibrium state. The main frequency of the free surface oscillation slightly increases with the increasing filling ratio and then nearly keeps constant in the range of low filling ratios. On the other hand, it increases monotonously with the increasing filling ratio in the range of high filling ratios. The critical damping type dominates the oscillations in the range of intermediate filling ratios. With the gravity reduction to low-gravity condition, the dynamic behavior of the free surface is qualitatively same. However, the residual gravity underdamping do results in significant differences in not only the equilibrium state of the ullage but also the temporal evolution of oscillation frequencies and magnitudes. Therefore, the effects of residual gravity level on the performance of the liquid storage tanks should be seriously considered for the future utilization design in space.

Acknowledgements This research is supported by the Key Research Program of Frontier Sciences, CAS (Grant No. QYZDY-SSWJSC040), the National Nature Science Foundation of China (Gant No. 11672311) and Strategic Project of Leading Science and Technology (class A), CAS (Grant No. XDA15012700).

References

Almohammadi, H., Amirfazli, A.: Droplet impact: viscosity and wettability effects on splashing. J Colloid Interface Sci. **553**, 22–30 (2019). https://doi.org/10.1016/j.jcis.2019.05.101

Blake, T.D., Batts, G.N.: The temperature-dependence of the dynamic contact angle. J Colloid Interface Sci. **553**, 108–116 (2019). https://doi.org/10.1016/j.jcis.2019.06.006

Brackbill, J.U., Kothe, D.B., Zemach, C.: A continuum method for modeling surface tension. J Comput Phys. **100**((2)), 335–354 (1992)

Chang, S., Ding, L., Song, M., Leng, M.: Numerical investigation on impingement dynamics and freezing performance of micrometer-sized water droplet on dry flat surface in supercooled environment. Int J Multiphase Flow. **118**, 150–164 (2019). https://doi.org/10.1016/j.ijmultiphaseflow.2019.06.011

Chiba, M., Magata, H.: Influence of liquid sloshing on dynamics of flexible space structures. J Sound Vib. **401**, 1–22 (2017). https://doi.org/10.1016/j.jsv.2017.04.029

Cox, R.G.: The dynamics of the spreading of liquids on a solid surface. Part 1. Viscous flow. J Fluid Mech. **168**, 169–194 (1986). https://doi.org/10.1017/S0022112086000332

Dai, J., Han, M., Ang, K.K.: Moving element analysis of partially filled freight trains subject to abrupt braking. Int J Mech Sci. **151**, 85–94 (2019). https://doi.org/10.1016/j.ijmecsci.2018.11.011

Dalmon, A., Lepilliez, M., Tanguy, S., Pedrono, A., Busset, B., Bavestrello, H., Mignot, J.: Direct numerical simulation of a bubble motion in a spherical tank under external forces and micro-gravity conditions. J Fluid Mech. **849**, 467–497 (2018). https://doi.org/10.1017/jfm.2018.389

Dalmon, A., Lepilliez, M., Tanguy, S., Alis, R., Popescu, E.R., Roumiguié, R., Miquel, T., Busset, B., Bavestrello, H., Mignot, J.: Comparison between the FLUIDICS experiment and direct numerical simulations of fluid sloshing in spherical tanks under microgravity conditions. Microgravity Sci Technol. **31**(1), 123–138 (2019). https://doi.org/10.1007/s12217-019-9675-4

Deng, M.L., Yue, B.Z.: Attitude tracking control of flexible spacecraft with large amplitude slosh. Acta Mech Sinica. **33**(6), 1095–1102 (2017). https://doi.org/10.1007/s10409-017-0700-9

Fernandez, J., Sanchez, P.S., Tinao, I., Porter, J., Ezquerro, J.M.: The CFVib experiment: control of fluids in microgravity with vibrations. Microgravity Sci Technol. **29**(5), 351–364 (2017). https://doi.org/10.1007/s12217-017-9556-7

Fricke, M., Koehne, M., Bothe, D.: A kinematic evolution equation for the dynamic contact angle and some consequences. Physica D-Nonlinear Phenomena. **394**, 26–43 (2019). https://doi.org/10.1016/j.physd.2019.01.008

Frosina, E., Senatore, A., Andreozzi, A., Fortunato, F., Giliberti, P.: Experimental and Numerical Analyses of the Sloshing in a Fuel Tank. Energies. **11**((3)), (2018). https://doi.org/10.3390/en11030682

Gueyffier, D., Li, J., Nadim, A., Scardovelli, R., Zaleski, S.: Volume-of-fluid interface tracking with smoothed surface stress methods for three-dimensional flows. J Comput Phys. **152**(2), 423–456 (1999)

Han, M., Dai, J., Wang, C.M., Ang, K.K.: Hydrodynamic analysis of partially filled liquid tanks subject to 3D vehicular Manoeuvring. Shock Vib. **2019**, 1–14 (2019). https://doi.org/10.1155/2019/6943879

Hasheminejad, S.M., Soleimani, H.: An analytical solution for free liquid sloshing in a finite-length horizontal cylindrical container filled to an arbitrary depth. Appl Math Model. **48**, 338–352 (2017). https://doi.org/10.1016/j.apm.2017.03.060

Hirt, C.W., Nichols, B.D.: Volume of fluid (VOF) method for the dynamics of free boundaries. J Comput Phys. **39**(1), 201–225 (1981)

Hoffman, R.L.: A study of the advancing interface, I. Interface shape in liquid—gas systems. J Colloid Interface Sci. **50**(2), 228–241 (1975)

Issa, R.I.: Solution of implicitly discretized fluid flow equations by operator splitting. J Comput Phys. **62**, 40–65 (1986)

Jiang, T.S., Soo-Gun, O.H., Slattery, J.C.: Correlation for dynamic contact angle. J Colloid Interface Sci. **69**(1), 74–77 (1979)

Kistler, S.F.: Hydrodynamics of wetting. in Wettability, edited by J. C. Berg (Marcel Dekker, New York, 1993), p.311 (1993)

Li, J.C., Lin, H., Zhao, J.-F., Li, K., Hu, W.-R.: Dynamic behaviors of liquid in partially filled tank in short-term microgravity. Microgravity Sci Technol. **30**(6), 849–856 (2018). https://doi.org/10.1007/s12217-018-9642-5

Luppes, R., Helder, J.A., Veldman, A.E.P.: The Numerical Simulation of Liquid Sloshing in Microgravity. In: Computational Fluid Dynamics 2006. pp. 607–612. (2009)

Malgarinos, I., Nikolopoulos, N., Marengo, M., Antonini, C., Gavaises, M.: VOF simulations of the contact angle dynamics during the drop spreading: standard models and a new wetting force model. Adv Colloid Interf Sci. **212**(3), 1–20 (2014)

Miao, N., Li, J., Wang, T.: Equivalent mechanical model of large-amplitude liquid sloshing under time-dependent lateral excitations

in low-gravity conditions. J Sound Vib. **386**, 421–432 (2017). https://doi.org/10.1016/j.jsv.2016.08.029

Ohayon, R., Soize, C.: Vibration of structures containing compressible liquids with surface tension and sloshing effects, Reduced-order model. Comput Mech. **55**(6), 1071–1078 (2015). https://doi.org/10.1007/s00466-014-1091-4

Popinet, S., Zaleski, S.: Simulation of Axisymmetric Free Surface Viscous Flow around a Non-spherical Bubble in the Sonoluminescence Regime. In, Third International Conference on Multiphase Flow (1998)

Quetzeri-Santiago, M.A., Yokoi, K., Castrejon-Pita, A.A., Castrejon-Pita, J.R.: Role of the Dynamic Contact Angle on Splashing. Phys Rev Lett. **122**((22)), (2019). https://doi.org/10.1103/PhysRevLett.122.228001

Sanapala, V.S., Rajkumar, M., Velusamy, K., Patnaik, B.S.V.: Numerical simulation of parametric liquid sloshing in a horizontally baffled rectangular container. J Fluids Struct. **76**, 229–250 (2018). https://doi.org/10.1016/j.jfluidstructs.2017.10.001

Scardovelli, R., Zaleski, S.: Direct Numerical Simulation of Free-Surface and Interfacial Flow. Annu Rev Fluid Mech. **31**((1)), 567–603 (1999)

Šikalo, Š., Wilhelm, H.D., Roisman, I.V., Jakirlić, S., Tropea, C.: Dynamic contact angle of spreading droplets: Experiments and simulations. Phys Fluids. **17**((6)), (2005). https://doi.org/10.1063/1.1928828

Snoeijer, J.H., Andreotti, B.: Moving contact lines: scales, regimes, and dynamical transitions. Annu Rev Fluid Mech. **45**(1), 269–292 (2013). https://doi.org/10.1146/annurev-fluid-011212-140734

Stange, M., Dreyer, M.E., Rath, H.J.: Capillary driven flow in circular cylindrical tubes. Phys Fluids. **15**(9), 2587–2601 (2003). https://doi.org/10.1063/1.1596913

Sui, Y., Ding, H., Spelt, P.D.M.: Numerical simulations of flows with moving contact lines. Annu Rev Fluid Mech. **46**(1), 97–119 (2014). https://doi.org/10.1146/annurev-fluid-010313-141338

Utsumi, M.: Slosh damping caused by friction work due to contact angle hysteresis. AIAA J. **55**(1), 265–273 (2017). https://doi.org/10.2514/1.j055238

Viola, F., Brun, P.T., Gallaire, F.: Capillary hysteresis in sloshing dynamics: aweakly nonlinear analysis. J Fluid Mech. **837**, 788–818 (2018). https://doi.org/10.1017/jfm.2017.860

Vreeburg, J.P.B.: Simulation of liquid dynamics onboard Sloshsat FLEVO. Paper presented at the AIP Conference Proceedings (1999). https://doi.org/10.1063/1.57704

Wang, J., Sun, S.L., Hu, J.: The coupling analysis of tank motion and sloshing by a fully nonlinear decoupling method. Nonlinear Dyn. **89**(2), 971–985 (2017). https://doi.org/10.1007/s11071-017-3495-0

Wang, X., Zhou, B., Jiang, M.: Technical challenges in numerical simulation of droplet behaviors with dynamic contact angle in microchannels. Int J Energy Res. **43**(9), 4828–4839 (2019). https://doi.org/10.1002/er.4633

Yang, W.J., Zhang, T.T., Li, C., Li, S.M., Xu, X.H.: Numerical Simulation of Pitching Sloshing under Microgravity. J Appl Fluid Mech. **12**((5)), 1527–1537 (2019). https://doi.org/10.29252/jafm.12.05.29677

Youngs, D.L.: Time-Dependent Multi-material Flow with Large Fluid Distortion. In: Morton, W., Baines, M.J. (eds.) Numerical Methods in Fluid Dynamics, pp. 273–285. Academic Press (1982)

Zhang, F., Zhang, X., Liu, Y.: An augmented incompressible material point method for modeling liquid sloshing problems. Int J Mech Mater Des. **14**(1), 141–155 (2018). https://doi.org/10.1007/s10999-017-9366-5

Zhao, D.Y., Hu, Z.Q., Chen, G., Chen, X.B., Feng, X.Y.: Coupling analysis between vessel motion and internal nonlinear sloshing for FLNG applications. J Fluids Struct. **76**, 431–453 (2018). https://doi.org/10.1016/j.jfluidstructs.2017.10.008